Article

Dissociative Adsorption and Thermal Evolution of Acetic Acid on Si(100)2×1: Surface-Mediated Formation of Ketene and Acetaldehyde from Unidentate and Bidentate Acetate Adsorbates

Maryam Ebrahimi, Jose Fernando Rios, and Kam Tong Leung

More About This Article

Additional resources and features associated with this article are available within the HTML version:

- Supporting Information
- Access to high resolution figures
- Links to articles and content related to this article
- Copyright permission to reproduce figures and/or text from this article

View the Full Text HTML

Dissociative Adsorption and Thermal Evolution of Acetic Acid on Si(100)2×1: Surface-Mediated Formation of Ketene and Acetaldehyde from Unidentate and Bidentate Acetate Adsorbates

Maryam Ebrahimi, Jose Fernando Rios, and Kam Tong Leung*

WATlab, and Department of Chemistry, University of Waterloo, Waterloo, Ontario N2L 3G1, Canada

Received: August 26, 2008; Revised Manuscript Received: November 4, 2008

The dissociative adsorption of acetic acid on Si(100)2×1 at room temperature has been investigated by X-ray photoelectron spectroscopy (XPS) and temperature-programmed desorption (TPD), as well as density-functional theory (DFT) calculations. The three C 1s features obtained by XPS measurement can be attributed to the carboxyl C of bidentate acetate (at 286.9 eV) and unidentate acetate (at 289.8 eV), resulting from O−H dissociation upon adsorption, and the methyl C (at 285.7 eV). Furthermore, the formation of bidentate acetate at a low exposure is found to be followed by that of unidentate acetate at a higher exposure, with approximately equal population for both adstructures at the saturation exposure. This is also supported by our DFT calculations, which show that the bidentate acetate adstructure is the most stable configuration among the calculated adstructures. The combined temperature-dependent XPS and TPD studies provide strong evidence for the formation of ketene, acetaldehyde, and CO, with almost half of the adstructures dissociated into methyl groups that become SiC with increasing annealing temperature to 933 K. We propose plausible surface-mediated reaction pathways that could account for these products. The present work indicates the pivotal importance of the 2×1 surface in facilitating the thermally driven formation of ketene and acetaldehyde from the acetate adstructures.

1. Introduction

Organic functionalization of semiconductor surfaces such as Si(100)2×1 has attracted a lot of recent attention,[1–10] due to its potential applications in organic−inorganic hybrid semiconductor devices, molecular electronics, chemical and biological sensors, and optical materials.[2,11–15] Understanding the behavior of organic molecules on the Si(100)2×1 surface is fundamentally important, because the electronic and chemical properties and selectivity of the inorganic substrate can be modified by the organic adsorbate.[2] The reactivity of the Si(100) surface comes from the two directional dangling bonds of individual surface atoms. Under appropriate preparation conditions, the Si(100) surface reconstructs to the 2×1 surface, on which the dangling bonds of the adjacent Si atoms pair up to create the surface dimer rows.[1,2,5,6] The dimer bond may be considered as comprising a full σ bond and a partial π bond, and it provides a unique reactive site for studying organosilicon chemistry. The reactivity of the Si═Si dimer in the pericyclic reactions such as the [2 + 2] and [4 + 2] cycloaddition reactions, of which stereochemistry can be predicted by the Woodward−Hoffmann rules,[16] has been demonstrated by many studies.[1–3,10] The asymmetric charge distribution in the $Si^{\delta+}$═$Si^{\delta-}$ dimer results in nucleophile and electrophile sites that ultimately control the reactivity and selectivity of the Si(100)2×1 surface.

Surface reactions on Si(100)2×1 have been reported for many organic molecules with single or multiple functional groups, including unsaturated aliphatic hydrocarbons (ethylene,[17–22] acetylene[18,22–24]), aromatic hydrocarbons (benzene[25–27]), halogenated hydrocarbons,[28–33] amines,[34–36] amino acids,[37,38] carbonyl compounds (aldehyde,[39,40] ketone[39,41]), alcohols,[42–46] and aliphatic and aromatic carboxylic acids (formic acid,[47–49] vinyl

acetic acid,[50] benzoic acid,[51,52] and 4-aminobenzoic acid[53]). Among the wide range of organic functional groups, the carboxyl group is one of the key constituents of amino acids, the building blocks of peptides and proteins. The interaction of the carboxyl group with the Si═Si dimers is therefore of special interest to understanding the chemical reactivity and selectivity of biomolecules in general with this widely used semiconductor.

Dissociative reactions of amines[34–36,54] and alcohols[43,44,46] with the dangling bonds of Si(100)2×1 at room temperature (RT) have been discussed in the literature. Formic acid, benzoic acid, and 4-aminobenzoic acid have also been found to dissociate through the O−H bond to form the unidentate formate, benzoate, and aminobenzoate on the Si(100)2×1 surface. Furthermore, unidentate vinyl acetate adstructure has been proposed by Hwang et al.[50] for the 2×1 surface, upon selective O−H dissociative reaction of vinyl acetic acid (a bifunctional unsaturated carboxylic acid) over the [2 + 2] C═C or C═O cycloaddition reaction. To date, no experimental study has been reported for the adsorption and thermal chemistry of acetic acid (the parent carboxylic acid from which glycine or α-amino acetic acid is derived) on Si(100)2×1. Of the two density functional theory (DFT) computational studies for acetic acid on the 2×1 surface, Kim and Cho[55] presented two adsorption pathways to illustrate that both unidentate acetate and the [2 + 2] C═O cycloaddition reaction product are energetically feasible. However, only the unidentate acetate adstructure is expected to remain on the Si dimers because desorption of the latter adstructure is easily activated at RT. In the other DFT study, Carbone and Cominiti[56] investigated several fragmentation pathways of the adstructures of acetic acid arising from the O−H and C−H bond cleavages. The resulting unidentate adstructure (obtained from O−H bond cleavage) becomes an intradimer bidentate acetate after the dissociated H atom has relocated onto

a neighboring dimer site. From the C—H bond breakage, the resulting adstructure could further fragment on the surface to a methyl and a carboxylic acid groups. The adsorption of acetic acid on a sister surface, Ge(100)2×1, at RT has been recently studied by Filler et al.,[57] Kim and co-workers,[58,59] and Kim and Cho.[60] In particular, by using scanning tunneling microscopy (STM)[59] and DFT calculations,[58,59] Kim and co-workers inferred the presence of both unidentate and "end-bridged" bidentate acetates on Ge(100)2×1 at RT, with the "on-top" bidentate acetate becoming feasible only after annealing to 400 K. (Kim and co-workers referred to the bonding of the carboxyl O atoms to two Ge atoms in two adjacent dimers as "end-bridged" bidentate and that to two Ge atoms in a single dimer as "on-top" bidentate.[58,59] In the present work, we refer to these adstructures, respectively, as interdimer bidentate[57] and intradimer bidentate.) The unidentate and "end-bridged" bidentate acetates have been earlier investigated by Filler et al. by using DFT, XPS, and Fourier transform infrared (FTIR) spectroscopy.[57] They also observed the conversion of bidentate acetate to unidentate acetate upon increasing coverage at RT, while an increase in the bidentate acetate signature was found after annealing the surface to 400 K. These studies highlighted the important role of the semiconductor surface in mediating selective reactions not found in wet chemistry.

In the present work, we investigate the adsorption of acetic acid on Si(100)2×1 and the thermal evolution of the adsorption products by using XPS and TPD. Our results show the formation of bidentate acetate at low exposure and of both unidentate and bidentate acetates at the saturation coverage, upon O—H dissociative adsorption of acetic acid on the 2×1 surface at RT. Our DFT calculations show that of the several energetically possible reaction products arising from [2 + 2] C=O cycloaddition, C—OH dissociation, and ene formation, the unidentate and bidentate acetates are the most stable adstructures. The adsorption behavior of acetic acid on the Si(100)2×1 surface observed in the present work is found to be different from that on Ge(100)2×1 reported earlier.[57] Our TPD results further reveal the formation of acetaldehyde and ketene from adsorbed acetate on Si(100)2 × 1 for the first time. In organic chemistry, the formation of aldehyde from carboxylic acid commonly involves a two-step process: reduction of carboxylic acid to primary alcohol, followed by its oxidation to aldehyde.[16] The development of new methods for producing ketene has also been of considerable interest due to the important role of ketene as a reactive intermediate in many reactions.[61] The present work shows a one-step process of generating acetaldehyde and ketene directly from the acetate adstructures on the Si(100)2×1 surface, suggesting that the 2×1 surface could be used as an important platform for discovering new synthesis methods.

2. Experimental and Computational Details

All the experiments were performed in a home-built dual-chamber ultrahigh vacuum system with a base pressure better than $1×10^{-10}$ Torr. The sample preparation chamber was equipped with an ion-sputtering gun, and a four-grid retarding-field optics for both reverse-view low energy electron diffraction and Auger electron spectroscopy. The XPS and TPD mass spectrometry studies were carried out in the analysis chamber. A 14×10 mm^2 substrate was cut from a single-side polished p-type B-doped Si(100) wafer (0.4 mm thick) with a resistivity of 0.0080−0.0095 Ω cm. The sample mounting and preparation procedures have been described in detail elsewhere.[27] It should be noted that the entire sample holder used in the present work has been rebuilt out of tantalum to further minimize any

environmental effects. The surface was cleaned in the preparation chamber by cycles of Ar$^+$ sputtering (20 mA emission current, 1.5 kV beam energy) for 20 min at RT followed by annealing to 900 K for 5 min. The sample was then flash-annealed to 1100 K for 20 s to obtain the 2×1 reconstructed surface. The cleanliness of the 2×1 surface was further affirmed by the sharpness of the electron diffraction pattern and by our XPS data that showed no significant contamination.

Acetic acid (99.9% purity), a colorless liquid under ambient condition, was purified by several freeze−pump−thaw cycles before exposure to the silicon surface through a variable leak valve. The high purity of the exposed chemical was confirmed by its cracking pattern obtained in situ. All exposures were performed at RT and reported in units of Langmuir (1 L = 10^{-6} Torr s), with the pressure monitored by an uncorrected ionization gauge. Saturation coverage was used for both the TPD and XPS experiments unless stated otherwise.

TPD studies were conducted by using a differentially pumped 1−300 amu quadrupole mass spectrometer (VG Quadrupole SXP Elite). A home-built programmable proportional-integral-differential temperature controller was used to provide linear temperature ramping at an adjustable heating rate, typically set at 3.5 K s^{-1}. The temperature was measured by using a type-K thermocouple (wrapped in a Ta foil) mechanically placed in good contact with the front face of the sample. The temperature scale was calibrated by the desorption maximum of recombinative H$_2$ desorption from the monohydrides. To ensure that the selected masses originate only from the species desorbing from the Si surface, the sample was positioned within 1 mm to the entrance (2 mm dia.) of the differentially pumped housing of the mass spectrometer. Unless stated otherwise, the desorption profiles have been smoothed by adjacent averaging for better clarity.

XPS experiments were performed by using an electron spectrometer (VG Scientific CLAM-2), consisting of a hemispherical analyzer of 100 mm mean radius and a triple-channeltron detector, with a twin-anode X-ray source that supplied unmonochromatic Al Kα radiation at 1486.6 eV photon energy. XPS spectra were collected with an acceptance angle of ±4° at normal emission from the silicon sample, and with a constant pass energy of 50 eV, giving an effective energy resolution of 1.4 eV full-width-at-half-maximum for the Si 2p photopeak. The binding energy scale of the XPS spectra has been calibrated to the Si 2p feature of the bulk at 99.3 eV. Spectral peak fitting based on residual minimization with Gaussian−Lorentzian lineshapes was performed by using the Casa XPS software. For temperature-dependent XPS measurements, the sample was flash-annealed to the preselected temperature and cooled back to RT before collecting the XPS spectra.

Electronic structure calculations were performed by using the DFT method[62] with the Gaussian 03 software package.[63] The employed hybrid B3LYP functional is composed of Becke's three-parameter gradient-corrected exchange functional[64] and the Lee−Yang−Parr correlation functional.[65] The DFT/B3LYP method has been shown to provide generally good agreement with the experimental data for the adsorption of many molecular systems on Si(100)2×1.[9] In the present calculations, we employed four basis sets, including 6−31G(d), 6−31+G(d), 6−31++G(d), and 6−31++G(d,p), all of which gave similar results for the optimized geometries and total energies (with the larger basis set providing a lower total energy). The interpretation of our results below is based on the largest basis set [6−31++G(d,p)]. In the present work, the Si(100)2×1
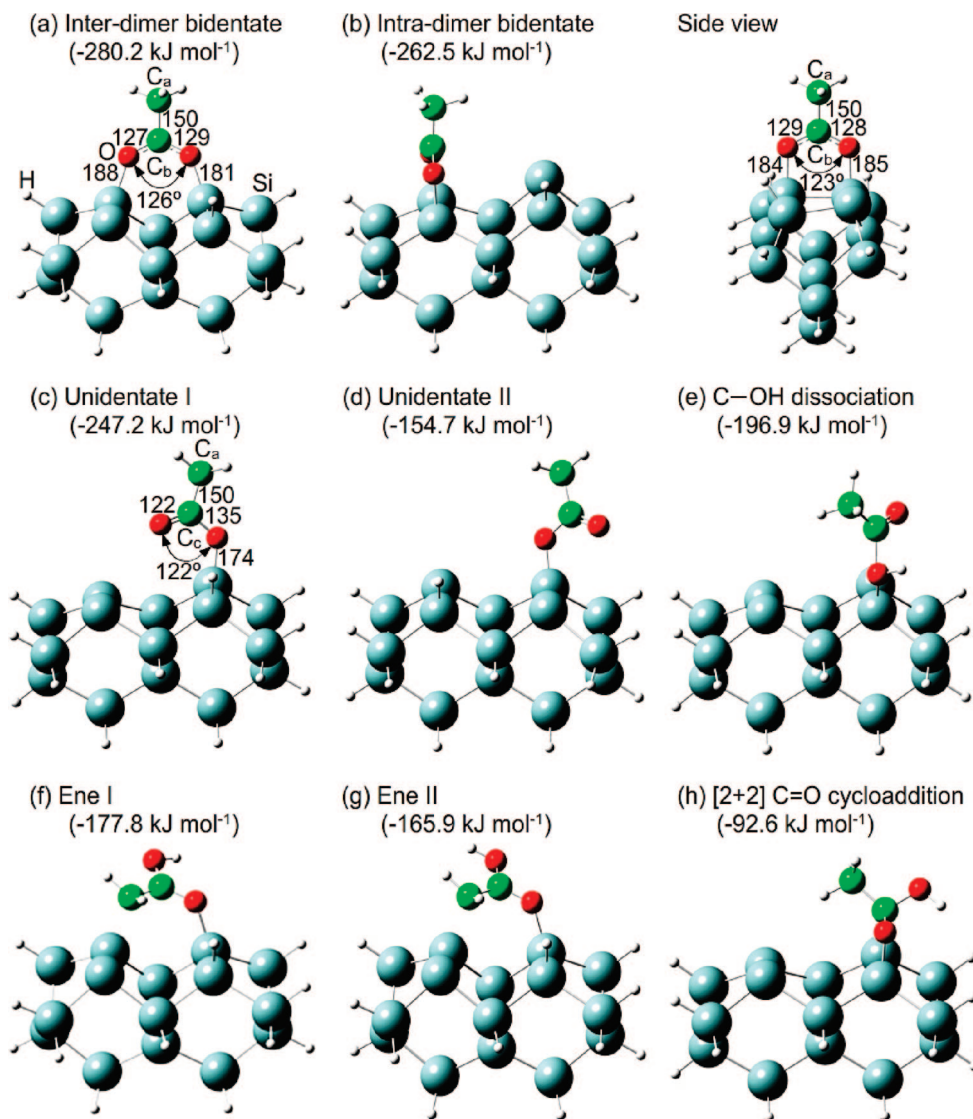
Figure 1. Optimized geometries of the adsorption structures of acetic acid on Si(100)2×1: (a) interdimer bidentate, (b) intradimer bidentate, (c) unidentate I, (d) unidentate II, (e) C−OH dissociation, (f) ene I, (g) ene II, and (h) [2 + 2] C═O cycloaddition reaction products. The corresponding adsorption energies (ΔE) calculated by 6−31++G(d,p) basis set are given in parentheses. All the bond lengths are in units of picometer.

surface was simulated by a double-dimer cluster of $Si_{15}H_{16}$. The adstructures of acetic acid were fully optimized without any geometrical constraint on the $Si_{15}H_{16}$ cluster. The corresponding adsorption energy (for acetic acid), ΔE, was estimated by the difference between the total energy for the optimized structures of the adsorbate−substrate configurations (ASCs) of the acetic acid adsorbate on the $Si_{15}H_{16}$ model surface and the sum of the total energies of a free acetic acid molecule and of a $Si_{15}H_{16}$ cluster. All the total energies were obtained without zero-point correction and no basis set superposition error correction was made to ΔE.

3. Results and Discussion

3.1. DFT Computational Study of Adsorbate−Substrate Configurations. Figure 1 shows eight possible adstructures on the double-dimer Si cluster model surface arising from (a, b, c, d) O−H dissociation, (e) C-OH dissociation, (f, g) ene reaction via C_α−H dissociation, and (h) [2 + 2] C═O cycloaddition, i.e. all with the CCO backbone intact. Frequency calculations for these ASCs (defined here as the optimized geometries for the combined adsorbate−$Si_{15}H_{16}$ structure) confirm their stabilities, with none being a transition state. Evidently, the four ASCs

(Figure 1e, 1f, 1g, 1h) resulting from the latter reactions are found to have discernibly less negative adsorption energies ΔE (and total energies) than the ASCs (Figure 1a, 1b, 1c) arising from O−H dissociation. In particular, the ΔEs for the interdimer bidentate ASC (-280.2 kJ mol^{-1}, Figure 1a) and intradimer bidentate ASC (-262.5 kJ mol^{-1}, Figure 1b) are more negative than the unidentate I ASC (-247.2 kJ mol^{-1}, Figure 1c). The formation of an additional Si−O bond in both bidentate ASCs (Figure 1a, 1b) leads to a more strongly adsorbed structure than the unidentate I ASC (Figure 1c). Furthermore, the less stable intradimer bidentate ASC, relative to the interdimer bidentate ASC, could be due to more strain in the Si−O−C bond angle (120° for the former ASC compared to 135° for the latter ASC, not shown in Figure 1). We also obtain a second unidentate II ASC involving the dissociated H atom and acetate bonded to two adjacent Si dimers (Figure 1d), instead of a single Si dimer as in unidentate I ASC (Figure 1c). This ASC (with $\Delta E = -154.7$ kJ mol^{-1}) is notably less stable, because, unlike the unidentate I ASC, it involves additional energy for relocating the dissociated H-atom to the closest dangling bond site of an adjacent Si dimer. For the optimized geometry of the unidentate I ASC shown in Figure 1c, the bond lengths for C−O and C═O

TABLE 1: Comparison of the Adsorption Energies ΔE and Total Energies (in square parentheses) for the Three Most Stable Adsorbate–Substrate Configurations (ASCs) of Acetic Acid on Si(100)2×1 Obtained by DFT/B3LYP Calculations with 6-31G(d), 6-31+G(d), 6-31++G(d), and 6-31++G(d,p) Basis Sets

ΔE (kJ mol⁻¹) [total energy (hartree)]	interdimer bidentate	intradimer bidentate	unidentate I
6−31G(d)	−311.7 [−4581.25958]	−294.7 [−4581.25309]	−274.0 [−4581.24522]
6−31+G(d)	−291.7 [−4581.27918]	−274.1 [−4581.27246]	−258.7 [−4581.26663]
6−31++G(d)	−291.6 [−4581.28073]	−274.0 [−4581.27399]	−258.8 [−4581.26820]
6−31++G(d,p)	−280.2 [−4581.30385]	−262.5 [−4581.29711]	−247.2 [−4581.29129]

are 135 and 122 pm, respectively. On the other hand, the bond lengths for both C··O bonds within the bidentate ASCs (Figure 1a, 1b) are ~128 pm, which lies between those of a single and a double bond. Our frequency calculation also reveals that the wavenumber found for this 11/2 C··O bond (1437−1560 cm⁻¹) in the bidentate ASCs is between those for the C−O (1265 cm⁻¹) and C=O bonds (1765 cm⁻¹) for the unidentate ASC. The relevant C−C and O−Si bond lengths and the O−C−O bond angle are also indicated in Figure 1. Table 1 summarizes the adsorption energies and total energies of the most stable ASCs (Figure 1a, 1b, 1c) obtained with the 6−31G(d), 6−31+G(d), 6−31++G(d), and 6−31++G(d,p) basis sets. It is of interest to compare the present adsorption energies with the corresponding energies for acetic acid on Ge(100) calculated by Kim and Cho.[60] In particular, their result shows that the stability of the calculated ASCs on Ge(100) follows a different order (intradimer bidentate > unidentate I > interdimer bidentate) than that reported here for Si(100).

3.2. XPS Study of the Adspecies at Room Temperature. Figure 2 shows the XPS spectrum of the C 1s region for a saturation exposure of acetic acid as deposited on Si(100)2×1 at RT, along with the more stable unidentate (unidentate I, Figure 2a) and bidentate (interdimer bidentate, Figure 2b) ASCs. The C 1s spectrum for the 100 L (saturation) exposure (Figure 2c) exhibits two broad bands. Three Gaussian profiles with an approximate full-width-at-half-maximum of 2.2 eV have been used in our curve-fitting procedure to identify the prominent C local chemical environments. In particular, the C 1s features at binding energies (BEs) of 285.7, 286.9, and 289.8 eV with respective relative intensities of 0.500, 0.247, and 0.253 (or

approximately 2:1:1) have been found. It should be noted that the corresponding XPS spectrum for a lower exposure (5 L) of acetic acid reveals only the band at the lower BE, which could be fitted with the first two features (with nearly equal intensities) of the spectrum obtained for the saturation exposure (Figure 2c).

In accord with our DFT calculations, the ASCs arising from O−H dissociation (Figure 1a, 1b, 1c) are the most stable (with the most negative ΔE values). Evidently, the chemical environments of the methyl carbon (C_a) in the three ASCs are very similar, while the carboxyl carbon in the bidentate ASCs (C_b, Figure 1a, 1b) is different from that in the unidentate ASC (C_c, Figure 1c). Given that the electronegativity follows the ordering: [16] Si (1.8) < H (2.1) < C (2.5) < O (3.5), the methyl carbon (C_a) is expected to be partially negatively charged and therefore would exhibit a lower C 1s BE than the carboxyl carbons (C_b and C_c). The C 1s feature at 285.7 eV (Figure 2c) can therefore be attributed to C_a. The attachment of the carboxyl carbon to the electronegative oxygen atoms through C=O and C−O gives the partial positive charge to C_b and C_c. In order to understand the difference between C_b and C_c, we show a schematic model for the conversion of unidentate ASC (Figure 2a) to the resonance structures of the interdimer bidentate ASC in Figure 2d. An electron located at the O site of the C=O group in the unidentate ASC (Structure I) combines with the electron in the Si dangling bond to form a new Si−O covalent bond, creating the bidentate ASC (Structure IIa). Electron delocalization in the OCO moiety leads to the other two resonance structures (Structures IIb and IIc), giving rise to the resulting hybrid resonance structure shown as Structure II (Figure 2b). Inclusion of the electron from the Si dangling bond in the
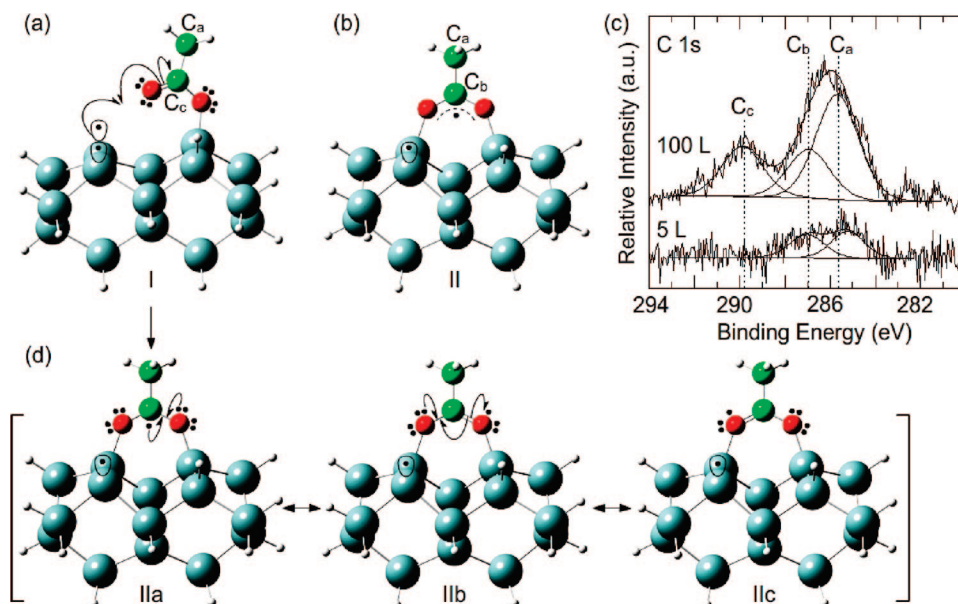

Figure 2. Schematic diagrams of (a) unidentate and (b) bidentate adstructures, and (d) the plausible resonance forms of the hybrid resonance structure (b). (c) XPS spectra of the C 1s region for a saturated exposure (100 L) and a 5-L exposure of acetic acid on Si(100)2×1 at 300 K.
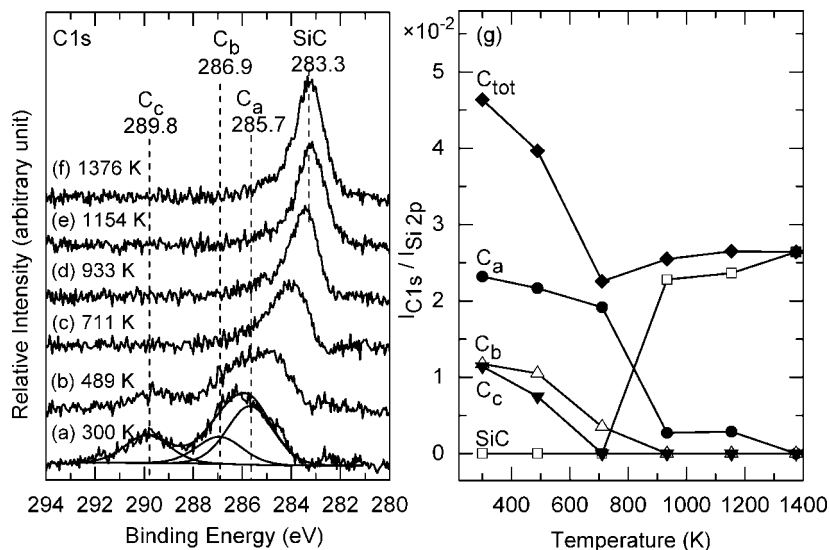
Figure 3. XPS spectra of the C 1s region for a saturated exposure of acetic acid on Si(100)2×1 (a) at 300 K, and upon sequential flash-annealing to (b) 489 K, (c) 711 K, (d) 933 K, (e) 1154 K, and (f) 1376 K. (g) Corresponding temperature profiles of the C 1s intensities ($I_{C\,1s}$) for SiC at 283.3 eV, C_a at 284.0−285.7 eV, C_b at 286.9 eV, and C_c at 289.8 eV, along with the total C 1s intensity (C_{tot}), all with respect to the intensity of Si 2p ($I_{Si\,2p}$).

formation of Structure II in effect reduces the partial positive charge of C_b, therefore lowering the corresponding BE. The C 1s features at 286.9 and 289.8 eV can be assigned to C_b and C_c, respectively. The observation of the lower-BE band (containing contributions from C_a and C_b) for the lower exposure indicates the preferred formation of the bidentate ASCs in the early stage of the adsorption process, which is consistent with the more negative adsorption energy (or ΔE) compared to that of the less stable unidentate ASC (Table 1).

The observed C 1s features at 285.7, 286.9, and 289.8 eV shown in Figure 2c can therefore be assigned to C_a, C_b, and C_c, respectively. Given the respective intensity ratio for C_a:C_b:C_c to be approximately 2:1:1, we conclude that the bidentate ASCs (including interdimer and/or intradimer ASCs) and unidentate I ASC must have nearly equal population. Hwang et al.[50] have also observed a similar double-peak C 1s spectrum for Si(100)2×1 saturated with vinyl acetic acid and assigned the higher-BE feature to the carboxyl C (C_3 in Figure 5 of ref 50) of the unidentate vinyl acetate. Furthermore, they attributed the lower-BE feature to the CH_2 (C_1 in Figure 5 of ref 50) and $H_2C=CH$ groups (C_2 in Figure 5 of ref 50), with the former appeared to have a notably higher fitted intensity than the latter, despite the expected stoichiometric ratio of 1:2. They also assigned the residual intensity in the lower-BE feature (C_4 in Figure 5 of ref 50) to the possible requirement for asymmetric lineshapes in the fitting and/or to surface contamination and other decomposition surface products. We believe that their resolved peak at the lower BE could be fitted alternatively such that C_3 and C_4 can be attributed respectively to the carboxyl C of the unidentate and bidentate adstructures. Furthermore, the stoichiometric ratio of 2:1 for C_2:C_1 in the unidentate and bidentate configurations should have been taken into account. In an investigation of the adsorption of formic acid on Si(111), Huang et al.[66] showed that the dissociation of formic acid to unidentate formate adstructure is consistent with the C 1s shift from 290.2 eV to a lower BE of 289.6 eV. Moreover, Baumann et al.[67] have observed a C 1s chemical shift of 2.7 eV for the carboxyl carbon from 290.7 eV for physisorbed acetic acid on Cu(110) also to a lower BE of 288 eV for its chemisorbed bidentate acetate. These latter studies provide indirect support

for our aforementioned C 1s assignment to the carbon atoms in the unidentate and bidentate adstructures.

3.3. XPS and TPD Studies of the Thermal Evolution of Adspecies. Figures 3 and 4 show the corresponding temperature-dependent XPS spectra of the C 1s and O 1s regions of a saturation exposure of acetic acid on Si(100)2×1, respectively. Evidently, the unidentate carboxyl C 1s peak at 289.8 eV (C_c) decreases in intensity upon annealing to 489 K (Figure 3b) and disappears completely after annealing to 711 K (Figure 3c). Similarly, the intensity of the bidentate carboxyl C 1s feature at 286.9 eV (C_b) also follows a similar decreasing trend and becomes totally extinguished at the annealing temperature of 933 K (Figure 3d). For the methyl C 1s peak at 285.7 eV (C_a), the peak position appears to shift to a lower BE (284.0 eV) while undergoing reduction in intensity upon annealing to 711 K (Figure 3c). This is followed by a dramatic reduction at the annealing temperature of 933 K (Figure 3d), at which a new feature at 283.3 eV that is commonly attributed to SiC is found to emerge. In Figure 3g, we summarize the observed intensity changes of these four C 1s features (C_a, C_b, C_c, and SiC) along with the total C 1s intensity, all relative to the intensity of Si 2p, as a function of the annealing temperature. Thermal evolution of the observed C 1s features therefore indicates that the carboxyl C (C_b, C_c) appears to have been removed from the surface at a temperature (~711 K) lower than that of the methyl C (C_a), which also suggests a C−C bond cleavage that leads to the direct attachment of the dissociated methyl group to the Si surface. Furthermore, unlike all of the carboxyl C that have apparently been totally removed at 711 K, the methyl group appears to remain on the surface and undergoes further dehydrogenation to eventually become SiC upon further annealing to 933 K. It is of interest to note that nearly half of the total C (corresponding to most of the carboxyl C and some of the methyl C) has left the surface upon annealing to 711 K, with the remaining being converted to SiC that cannot be removed even at an annealing temperature of 1376 K.

In Figure 4a, a broad O 1s feature at 532.7 eV is observed for a saturation exposure of acetic acid on Si(100)2×1 at RT. The observed O 1s BE position is in good accord with those of Si−O (531.9 eV) and C=O (532.8 eV) reported for vinyl acetic
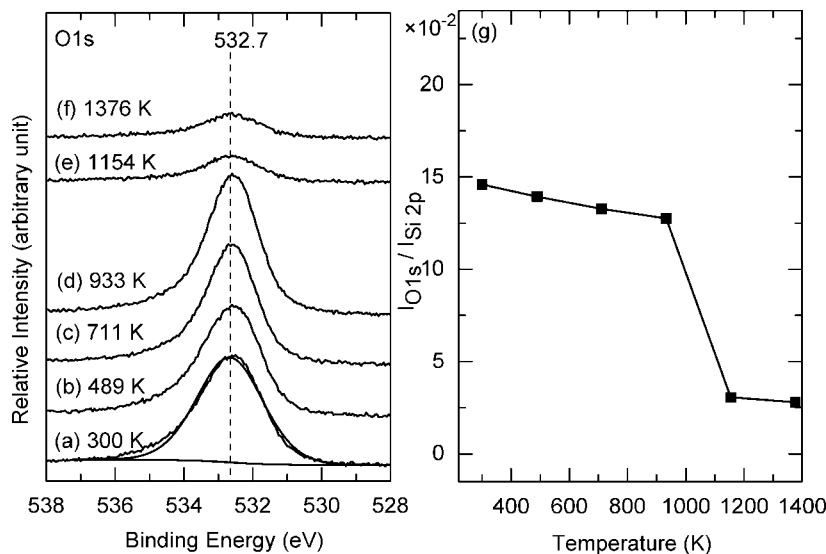
Figure 4. XPS spectra of the O 1s region for a saturated exposure of acetic acid on Si(100)2×1 (a) at 300 K, and upon sequential flash-annealing to (b) 489 K, (c) 711 K, (d) 933 K, (e) 1154 K, and (f) 1376 K. (g) Corresponding temperature profile of the O 1s intensity ($I_{O\ 1s}$) with respect to the intensity of Si 2p ($I_{Si\ 2p}$).

acid.[50] Upon annealing to 933 K (Figure 4d), the O 1s feature is found to undergo a slight reduction in intensity and become sharper, suggesting that the O-containing adspecies are becoming more homogeneous on the surface as other adspecies are desorbed from the surface with increasing annealing temperature. The O 1s feature becomes greatly reduced at 1154 K (Figure 4e), which evidently is higher than the temperature at which most of the carboxyl C 1s feature is removed (711−933 K, Figure 3g). This suggests that unidentate and bidentate acetates fragment on the surface into adspecies (to be discussed below) that desorb at 489−933 K, and individual O atoms that desorb from the surface above 1000 K (likely as SiO) or diffuse into the bulk. Finally, the residual O 1s intensity above 1154 K likely corresponds to thermal oxides (Figure 4g).

In addition to the temperature-dependent XPS spectra that show the adspecies remaining on the 2×1 surface after the sample has been annealed to different temperatures, we also perform TPD experiments to investigate the desorption products evolving from the surface as a function of temperature. Figure 5 shows the TPD profiles of selected mass fragments with m/z 2, 15, 28, 29, 42, 43, and 44 for a RT saturation exposure of acetic acid on Si(100)2×1. We also monitor other mass fragments, including m/z 60 and 45 corresponding to the parent mass (CH_3COOH^+) and $COOH^+$ fragment of acetic acid[68] respectively, all of which do not exhibit any notable TPD features, suggesting no molecular adsorption of acetic acid at RT. For m/z 2, a large desorption feature at 810 K is observed (Figure 5a), which is consistent with the recombinative desorption of H_2 from silicon monohydride.[69] The TPD feature with the next highest intensity is observed at 625 K for m/z 28 (Figure 5c), which corresponds to the parent mass of CO. The TPD features for the remaining mass fragments all appear to have notably smaller relative intensities. In particular, m/z 42 corresponds to the parent mass of ketene, $CH_2=C=O$, the cracking pattern of which also contains m/z 41 and 14 with substantial intensities.[68] The corresponding TPD profile (Figure 5e) exhibits a maximum at 580 K. Desorption maxima have been found to be near the same temperature of 565 K for the TPD profiles of m/z 44 (parent mass), 43, 29 (base mass), and 15 (Figure 5), all of which correspond to the cracking pattern of acetaldehyde CH_3CHO.[68] Furthermore, m/z 44 could also correspond to the parent/base mass of CO_2.
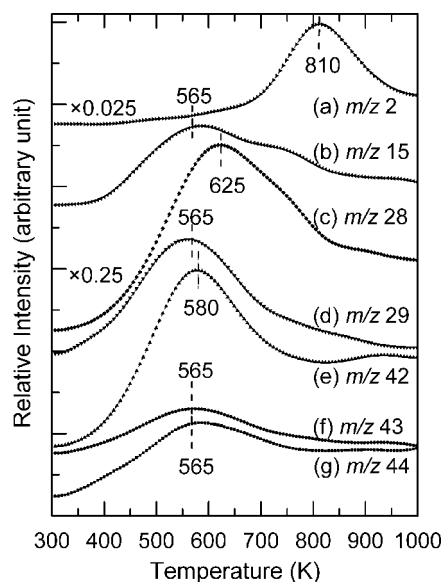

Figure 5. TPD profiles of selected fragments of m/z (a) 2, (b) 15, (c) 28, (d) 29, (e) 42, (f) 43, and (g) 44 for a saturation exposure of acetic acid on Si(100)2×1 at 300 K.

In Figure 6, we show plausible mechanisms for the formation of ketene and acetaldehyde from the unidentate acetate adspecies induced by thermal annealing. In particular, the unidentate acetate (Structure I) undergoes an elimination reaction of $CH_2=C=O$, upon nucleophilic attack of the bonded O atom on a methyl H atom (Figure 6a, Ia), with the resulting surface byproducts of H and OH. The adsorbed unidentate acetate could also thermally evolve to CH_3CHO by elimination of an adsorbed H atom after C−O bond cleavage, leaving the O atom on the surface (Figure 6b, Ib). In addition, breakage of C−C and C−O bonds in the acetate could produce dissociated methyl group, O and H atoms on the surface, generating the observed CO desorbate (Figure 6c, Ic). On the other hand, breakage of the C−C and Si−O bonds of the adstructure would also lead to dissociated methyl group and H atoms on the surface and CO_2 as the desorbate (Figure 6d, Id). Carbon dioxide could also in principle be generated from breakage of two Si−O bonds, in addition to the C−C bond (Figure 6e, IIa), in the adsorbed
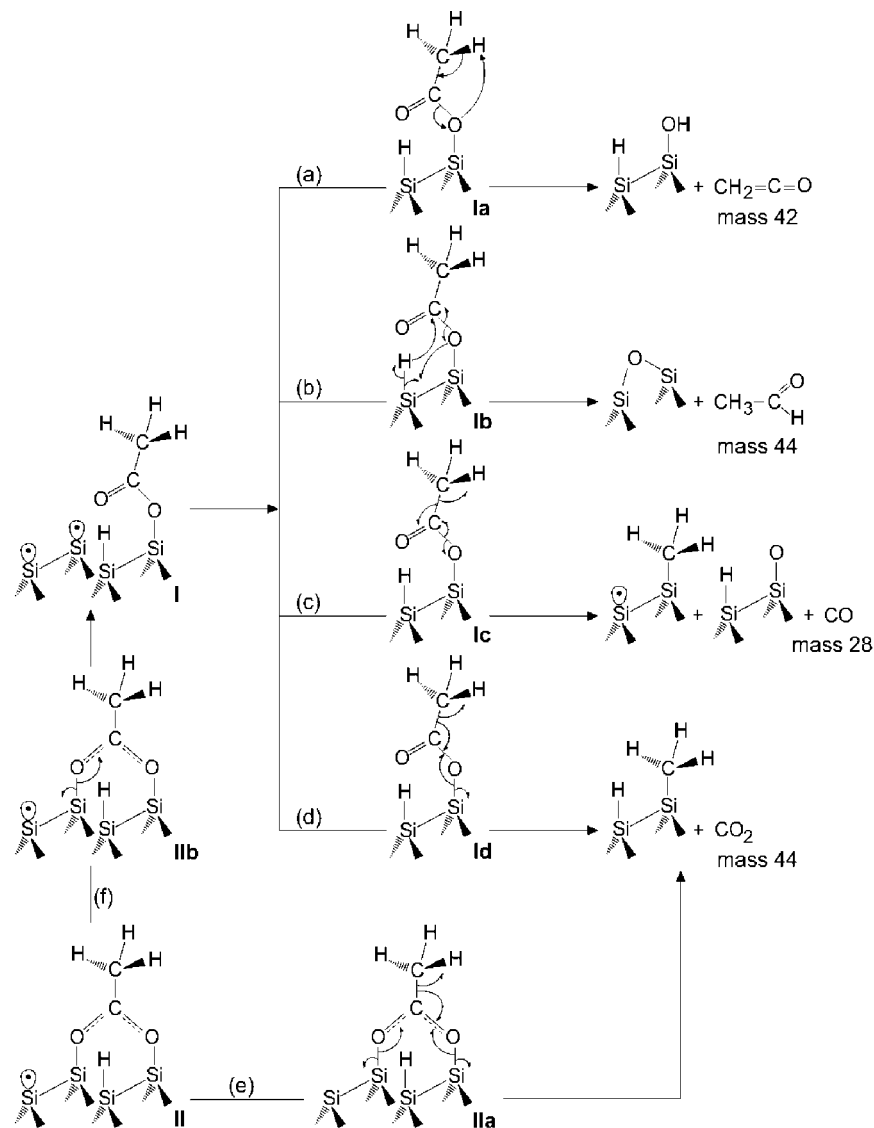
Surface-Mediated Formation of Ketene and Acetaldehyde

J. Phys. Chem. C, Vol. 113, No. 1, 2009 **287**

Figure 6. Schematic models for thermal evolution of unidentate acetate (structure I) and bidentate acetate (structure II), depicting the formation of (a) ketene, (b) acetaldehyde, (c) CO, and (d,e) CO_2 desorbates, and (f) their interconnection.

bidentate acetate (Structure II). The bidentate acetate can also convert to unidentate acetate via a single Si–O bond cleavage (Figure 6f, IIb). It should be noted that interconversion among dissociated H, O, and OH groups on the surface produced in the proposed pathways (Figures 6a, 6c) and the Si_2O structure (Figure 6b) could also occur.

The desorption maximum for CO or m/z 28 (625 K, Figure 5c) is slightly higher than ketene (580 K, Figure 5e) and acetaldehyde (565 K, Figure 5b, 5d, 5f, 5g). This indicates that there could be an additional desorption state at a higher temperature than 565 K, thus shifting the desorption maximum to 625 K. This observation is consistent with the proposed mechanism for CO formation from the unidentate acetate (Figure 6c) that requires nearly the same energy (844 kJ mol^{-1}) to break the necessary bonds, in comparison to those for the formation of ketene (858 kJ mol^{-1}, Figure 6a) and acetaldehyde (752 kJ mol^{-1}, Figure 6b). It should be noted that the typical bond dissociation energies (in kJ mol^{-1}) are 310 for Si–Si, 800 for Si–O, 447 for Si–C, 293 for Si–H, 459 for C–O, 385 for C–C, 399 for C–H, and 469 for O–H.[70] The considerably stronger intensity observed for the m/z 28 therefore suggests that the pathway for CO formation is kinetically favored on the 2×1 surface. Despite the discernibly smaller desorption

intensities observed for the ketene and acetaldehyde formation, it is important to emphasize that the Si(100)2×1 surface plays a pivotal role in mediating such types of thermally induced surface reactions. The conversion from bidentate to unidentate acetate requires breakage of a Si–O bond (800 kJ mol^{-1}), as depicted in Figure 6f, which could occur during the thermal evolution process, providing an additional source for unidentate acetate. The latter supply could account for the generally broad TPD profiles (with possible additional desorption state) that are found to extend into higher temperature.

It should be noted that there has been some ambiguity in the observation of CO_2 desorption from unidentate and bidentate organic adstructures. In their EELS and TPD study of the adsorption of formic acid on Si(100)2×1, Nishijima and co-workers[47] have commented that only 10% of the unidentate formate has dissociated to CO and CO_2. Later, the same group reported strong evidence of desorption of CO but not CO_2 from their TPD data.[48] Recently, a TPD and FTIR study of the adsorption of formaldehyde on Ge(100)2×1 by Filler et al.[71] has reported CO_2 desorption, which led the authors to propose the formation of a bidentate formate adstructure by a "carbon–oxygen coupling" mechanism. Given that the energy required for bond breaking in CO_2 production (1185 kJ mol^{-1}) is higher

than that for CO formation, the desorption for m/z 44 is expected to occur at a higher temperature (than 565–625 K) in the present work. However, the observed desorption maximum for m/z 44 occurs at 565 K, essentially identical to those found for m/z 43, 29, and 15 as part of the cracking pattern of acetaldehyde (Figure 5). We could therefore rule out the direct CO_2 formation pathway from unidentate acetate (Figure 6d) and attribute the observed m/z 44 as part of the acetaldehyde evolution. Furthermore, the formation of CO_2 from bidentate acetate, as proposed in Figure 6e, requires additional Si–O bond breaking and therefore an even larger bond breaking energy than the unidentate route (Figure 6d), which also makes this pathway improbable.

Our TPD results are consistent with our temperature-dependent XPS data. The reduction of the carboxyl C 1s XPS features in both unidentate and bidentate adstructures at 489–911 K occurs in the same temperature region (400–750 K) as the formation of ketene (Figure 6a) and acetaldehyde (Figure 6b) as well as CO (Figure 6c). For CO, there is evidently a clear shoulder (with substantial intensity) at 750 K in the m/z 28 TPD profile (Figure 5c). This suggests the continued production of CO desorbate and the surface methyl C as indicated in Figure 6c after the evolution to ketene and acetaldehyde. The observed gradual shift in the methyl C 1s XPS feature to that of SiC supports the gradual dissociation of the methyl group to C and H atoms with increasing temperature above 711 K. With the H atoms so produced undergoing recombinative H_2 desorption at 700–1000 K (Figure 5a), the remaining methyl C is being converted to SiC.

In the case of acetic acid on Ge(100)2×1, Filler et al.[57] presented a DFT calculation that showed that the unidentate acetate adstructure is slightly more stable than the bidentate acetate adstructure (by 2.2 kcal mol^{-1} or 9.2 kJ mol^{-1}), using a $Ge_4Si_{11}H_{16}$ cluster as the model for the Ge(100)2×1 surface. Furthermore, their IR data revealed the presence of both unidentate and bidentate adstructure at RT (while their XPS data could not resolve the C 1s feature for the bidentate), and the conversion of bidentate to unidentate with increasing exposure above 0.03 L. They also concluded that increased conversion of unidentate to bidentate adstructure occurred upon annealing to ∼400 K, for a saturation coverage of acetic acid on Ge(100)2×1. In contrast, the present work provides evidence of bidentate acetate (in addition to the unidentate acetate) on Si(100)2×1 from our XPS data for the first time. Our data show adsorption of bidentate acetate at a lower exposure than that of the unidentate acetate but no direct conversion of bidentate to unidentate adstructure at RT.

4. Summary

XPS and TPD experiments have been performed for the first time on acetic acid on Si(100)2×1. Of the eight ASCs considered here, DFT calculations show that the bidentate acetate gives the most stable ASCs, followed by the unidentate acetate ASCs. XPS spectra collected at different exposures demonstrate the preferred formation of bidentate ASC at a low exposure, followed by the unidentate ASC formation at a higher exposure, which therefore confirms the relative stabilities of the bidentate and unidentate ASCs. The observation of a more stable bidentate ASC on Si(100)2×1 is in good accord with those observed for a metal surface but in contrast to that found for Ge(100)2×1. Furthermore, the combined temperature-dependent XPS and TPD data reveal several plausible thermal evolution pathways that lead to the formation of ketene, acetaldehyde, and CO, with almost half of the ASCs dissociated into methyl

groups that become SiC with increasing annealing temperature to 933 K. These thermally induced reactions indicate the essential role of the 2×1 surface in mediating the formation of ketene and acetaldehyde. The directional dangling bonds on the Si(100)2×1 surface therefore provide a unique testing ground to investigate novel silicon organic chemistry. As one of the most fundamental biological molecules, acetic acid provides an important reference for studying more complex carboxyl-containing molecules, including amino acids. With the carboxyl group serving as the main anchor to the Si surface, derivatives of acetic acid with multiple functional groups can be used effectively as a linker molecule to further functionalize the Si(100)2×1 surface.

References and Notes

(1) Filler, M. A.; Bent, S. F. *Prog. Surf. Sci.* **2003**, *73*, 1–56.
(2) Bent, S. F. *Surf. Sci.* **2002**, *500*, 879–903.
(3) Hamers, R. J.; Coulter, S. K.; Ellison, M. D.; Hovis, J. S.; Padowitz, D. F.; Schwartz, M. P.; Greenlief, C. M.; Russell Jr, J. N. *Acc. Chem. Res.* **2000**, *33*, 617–624.
(4) Wolkow, R. A. *Annu. Rev. Phys. Chem.* **1999**, *50*, 413–441.
(5) Waltenburg, H. N.; Yates, J. T., Jr. *Chem. Rev.* **1995**, *95*, 1589–1673.
(6) Hamers, R. J.; Wang, Y. *Chem. Rev.* **1996**, *96*, 1261–1290.
(7) Buriak, J. M. *Chem. Commun.* **1999**, 1051–1060.
(8) Buriak, J. M. *Chem. Rev.* **2002**, *102*, 1271–1308.
(9) Lu, X.; Lin, M. C. *Int. Rev. Phys. Chem.* **2002**, *21*, 137–184.
(10) Leftwich, T. R.; Teplyakov, A. V. *Surf. Sci. Rep.* **2008**, *63*, 1–71.
(11) Kasemo, B. *Surf. Sci.* **2002**, *500*, 656–677.
(12) Yates, J. T., Jr. *Science* **1998**, *279*, 335–336.
(13) Lin, Z.; Strother, T.; Cai, W.; Cao, X.; Smith, L. M.; Hamers, R. J. *Langmuir* **2002**, *18*, 788–796.
(14) Stewart, M. P.; Buriak, J. M. *Comments Inorg. Chem.* **2002**, *23*, 179–203.
(15) Guisinger, N. P.; Greene, M. E.; Basu, R.; Baluch, A. S.; Hersam, M. C. *Nano Lett.* **2004**, *4*, 55–59.
(16) Carey, F. A. *Organic Chemistry*, 3rd ed.; McGraw-Hill: Toronto, 1996.
(17) Yoshinobu, J.; Tsuda, H.; Onchi, M.; Nishijima, M. *J. Chem. Phys.* **1987**, *87*, 7332–7340.
(18) Cheng, C. C.; Wallace, R. M.; Taylor, P. A.; Choyke, W. J.; Yates, J. T., Jr. *J. Appl. Phys.* **1990**, *67*, 3693–3699.
(19) Clemen, L.; Wallace, R. M.; Taylor, P. A.; Dresser, M. J.; Choyke, W. J.; Weinberg, W. H.; Yates, J. T., Jr. *Surf. Sci.* **1992**, *268*, 205–216.
(20) Mayne, A. J.; Avery, A. R.; Knall, J.; Jones, T. S.; Briggs, G. A. D.; Weinberg, W. H. *Surf. Sci.* **1993**, *284*, 247–256.
(21) Ikeda, M.; Maruoka, T.; Nagashima, N. *Surf. Sci.* **1998**, *416*, 240–244.
(22) Liu, H.; Hamers, R. J. *Surf. Sci.* **1998**, *416*, 354–362.
(23) Taylor, P. A.; Wallace, R. M.; Cheng, C. C.; Weinberg, W. H.; Dresser, M. J.; Choyke, W. J.; Yates, J. T., Jr. *J. Am. Chem. Soc.* **1992**, *114*, 6754–6760.
(24) Nishijima, M.; Yoshinobu, J.; Tsuda, H.; Onchi, M. *Surf. Sci.* **1987**, *192*, 383–397.
(25) Taguchi, T. Y.; Fujisawa, M.; Takaoka, T.; Okada, T.; Nishijima, M. *J. Chem. Phys.* **1991**, *95*, 6870–6876.
(26) Lopinski, G. P.; Fortier, T. M.; Moffatt, D. J.; Wolkow, R. A. *J. Vac. Sci. Technol. A* **1998**, *16*, 1037–1042.
(27) Li, Q.; Leung, K. T. *Surf. Sci.* **2001**, *479*, 69–82.
(28) Zhou, X. J.; Li, Q.; He, Z. H.; Yang, X.; Leung, K. T. *Surf. Sci.* **2003**, *543*, L668–L674.
(29) Naumkin, F. Y.; Polanyi, J. C.; Rogers, D. *Surf. Sci.* **2003**, *547*, 335–348.
(30) Zhou, X. J.; Leung, K. T. *Surf. Sci.* **2006**, *600*, 3285–3296.
(31) Zhou, X. J.; Li, Q.; Leung, K. T. *J. Phys. Chem. B* **2006**, *110*, 5602–5610.

Surface-Mediated Formation of Ketene and Acetaldehyde

J. Phys. Chem. C, Vol. 113, No. 1, 2009 **289**

(32) Zhou, X. J.; Leung, K. T. *J. Phys. Chem. B* **2006**, *110*, 9601–9607.

(33) Zhou, X. J.; He, Z. H.; Leung, K. T. *Surf. Sci.* **2006**, *600*, 468–477.

(34) Hlil, E. K.; Kubler, L.; Bischoff, J. L.; Bolmont, D. *Phys. Rev. B* **1987**, *35*, 5913–5916.

(35) Bozso, F.; Avouris, Ph. *Phys. Rev. B* **1988**, *38*, 3937–3942.

(36) Wu, J.-B.; Yang, Y.-W.; Lin, Y.-F.; Chiu, H.-T. *J. Phys. Chem. B* **2004**, *108*, 1677–1685.

(37) Lopez, A.; Heller, T.; Bitzer, T.; Richardson, N. V. *Chem. Phys.* **2002**, *277*, 1–8.

(38) Ferraz, A. C.; Miotto, R. *Brazilian J. Phys.* **2006**, *36*, 309–312.

(39) Armstrong, J. L.; White, J. M.; Langell, M. *J. Vac. Sci. Technol. A* **1997**, *15*, 1146–1154.

(40) Lu, X.; Zhang, Q.; Lin, M. C. *Phys. Chem. Chem. Phys.* **2001**, *3*, 2156–2161.

(41) Ferraz, A. C.; Miotto, R. *Appl. Surf. Sci.* **2004**, *234*, 185–189.

(42) Shannon, C.; Campion, A. *Surf. Sci.* **1990**, *227*, 219–223.

(43) Casaletto, M. P.; Zanoni, R.; Carbone, M.; Piancastelli, M. N.; Aballe, L.; Weiss, K.; Horn, K. *Surf. Sci.* **2002**, *505*, 251–259.

(44) Eng, J., Jr.; Raghavachari, K.; Struck, L. M.; Chabal, Y. J.; Bent, B. E.; Flynn, G. W.; Christman, S. B.; Chaban, E. E.; Williams, G. P.; Radermacher, K.; Mantl, S. *J. Chem. Phys.* **1997**, *106*, 9889–9898.

(45) Silvestrelli, P. L. *Surf. Sci.* **2004**, *552*, 17–26.

(46) Casaletto, M. P.; Zanoni, R.; Carbone, M.; Piancastelli, M. N.; Aballe, L.; Weiss, K.; Horn, K. *Surf. Sci.* **2000**, *447*, 237–244.

(47) Tanaka, S.; Onchi, M.; Nishijima, M. *J. Chem. Phys.* **1989**, *91*, 2712–2725.

(48) Kubo, T.; Minami, N.; Aruga, T.; Takagi, N.; Nishijima, M. *J. Phys. Chem. B* **1997**, *101*, 7007–7011.

(49) Ikeura-Sekiguchi, H.; Sekiguchi, T. *Surf. Sci.* **1999**, *433−435*, 549–553.

(50) Hwang, H.-N.; Baik, J. Y.; An, K.-S.; Lee, S. S.; Kim, Y.; Hwang, C. C.; Kim, B. *J. Phys. Chem. B* **2004**, *108*, 8379–8384.

(51) Bitzer, T.; Alkunshalie, T.; Richardson, N. V. *Surf. Sci.* **1996**, *368*, 202–207.

(52) Bitzer, T.; Richardson, N. V. *Surf. Sci.* **1999**, *427−428*, 369–373.

(53) Lopez, A.; Bitzer, T.; Heller, T.; Richardson, N. V. *Surf. Sci.* **2001**, *480*, 65–72.

(54) Mui, C.; Han, J. H.; Wang, G. T.; Musgrave, C. B.; Bent, S. F. *J. Am. Chem. Soc.* **2002**, *124*, 4027–4038.

(55) Kim, H.-J.; Cho, J.-H. *Phys. Rev. B* **2005**, *72*, 195305−1−195305−5.

(56) Carbone, M.; Caminiti, R. *Surf. Sci.* **2008**, *602*, 852–858.

(57) Filler, M. A.; Van Deventer, J. A.; Keung, A. J.; Bent, S. F. *J. Am. Chem. Soc.* **2006**, *128*, 770–779.

(58) Kim, D. H.; Hwang, E.; Hong, S.; Kim, S. *Surf. Sci.* **2006**, *600*, 3629–3632.

(59) Hwang, E.; Kim, D. H.; Hwang, Y. J.; Kim, A.; Hong, S.; Kim, S. *J. Phys. Chem. C* **2007**, *111*, 5941–5945.

(60) Kim, H.-J.; Cho, J.-H. *J. Phys. Chem. C* **2008**, *112*, 6947–6952.

(61) Seikaly, H. R.; Tidwell, T. T. *Tetrahedron* **1986**, *42*, 2587–2613.

(62) Kohn, W.; Sham, L. J. *Phys. Rev.* **1965**, *140*, A1133–A1138.

(63) Frisch, M. J.; Trucks, G. W.; Schlegel, H. B.; Scuseria, G. E.; Robb, M. A.; Cheeseman, J. R.; Montgomery J. A., Jr.; Vreven, T.; Kudin, K. N.; Burant, J.C.; Millam, J. M.; Iyengar, S. S.; Tomasi, J.; Barone, V.; Mennucci, B.; Cossi, M.; Scalmani, G.; Rega, N.; Petersson, G. A.; Nakatsuji, H.; Hada, M.; Ehara, M.; Toyota, K.; Fukuda, R.; Hasegawa, J.; Ishida, M.; Nakajima, T.; Honda, Y.; Kitao, O.; Nakai, H.; Klene, M.; Li, X.; Knox, J. E.; Hratchian, H. P.; Cross, J. B.; Bakken, V.; Adamo, C.; Jaramillo, J.; Gomperts, R.; Stratmann, R. E.; Yazyev, O.; Austin, A. J.; Cammi, R.; Pomelli, C.; Ochterski, J. W.; Ayala, P. Y.; Morokuma, K.; Voth, G. A.; Salvador, P.; Dannenberg, J. J.; Zakrzewski, V. G.; Dapprich, S.; Daniels, A. D.; Strain, M. C.; Farkas, O.; Malick, D. K.; Rabuck, A. D.; Raghavachari, K.; Foresman, J. B.; Ortiz, J. V.; Cui, Q.; Baboul, A. G.; Clifford, S.; Cioslowski, J.; Stefanov, B. B.; Liu, G.; Liashenko, A.; Piskorz, P.; Komaromi, I.; Martin, R. L.; Fox, D. J.; Keith, T.; Al-Laham, M. A.; Peng, C. Y.; Nanayakkara, A.; Challacombe, M.; Gill, P. M. W.; Johnson, B.; Chen, W.; Wong, M. W.; Gonzalez, C.; Pople, J. A. Gaussian 03, Gaussian, Inc., Wallingford, CT, 2005.

(64) Becke, A. D. *J. Chem. Phys.* **1993**, *98*, 5648–5652.

(65) Lee, C.; Yang, W.; Parr, R. G. *Phys. Rev. B* **1988**, *37*, 785–789.

(66) Huang, J. Y.; Huang, H. G.; Lin, K. Y.; Liu, Q. P.; Sun, Y. M.; Xu, G. Q. *Surf. Sci.* **2004**, *549*, 255–264.

(67) Baumann, P.; Bonzel, H. P.; Pirug, G.; Werner, J. *Chem. Phys. Lett.* **1996**, *260*, 215–222.

(68) NIST Mass Spec Data Center. Stein, S. E. Mass Spectra In *NIST Chemistry WebBook, NIST Standard Reference Database Number 69*, Linstrom, P. J., Mallard, W. G., Eds.; June 2005; National Institute of Standards and Technology: Gaithersburg, MD (http://webbook.nist.gov).

(69) Cheng, C. C.; Yates, J. T., Jr. *Phys. Rev. B* **1991**, *43*, 4041–4045.

(70) Luo, Y.-R. Bond Dissociation Energies In *CRC Handbook of Chemistry and Physics*, 88th ed.; Lide, D. R., Ed.; CRC Press/Taylor and Francis: Boca Raton, 2008.

(71) Filler, M. A.; Musgrave, C. B.; Bent, S. F. *J. Phys. Chem. C* **2007**, *111*, 1739–1746.